

Improved Imaged-derived Input Function for Study of Human Brain FDG-PET

Hongbin Guo

Arizona State University, Department of Mathematics

Tempe, AZ 85287-1804

Tel: 480-965-8002, Fax: 480-965-8119

Email: hb_guo@asu.edu

Rosemary Renaut

Arizona State University, Department of Mathematics

Tempe, AZ 85287-1804

Email: renaut@asu.edu

Kewei Chen

Positron Emission Tomography Center

Banner Good Samaritan Medical Center

Phoenix, AZ 85006

Email: kchen@math.la.asu.edu

This work was partially supported by the Arizona Center for Alzheimer's
Disease Research which is funded by the Arizona Department of Health
Services, and by NIH grant EB 2553301.

Improved Imaged-derived Input Function for Study of Human Brain FDG-PET

Hongbin Guo ^{a,*}Rosemary Renaut ^a Kewei Chen ^b

^a*Arizona State University, Department of Mathematics, Tempe, AZ 85287-1804*

^b*Positron Emission Tomography Center, Banner Good Samaritan Medical Center,
Phoenix, AZ 85006*

Abstract

A reliable, semi-automated method for estimation of a non-invasive image-derived input function is proposed and evaluated for human [¹⁸F]-fluoro deoxyglucose (FDG) positron emission tomography (PET) studies. The method recognizes two phases of the average time activity curves (TAC) of blood regions of interest (ROIs): an early period of rapid change followed by an interval of slow change. During the first phase the dominant contamination of the measured TAC, which is extracted from the imaged carotid artery (CA) region of interest, is due to partial volume effects. The second phase, however, is affected by both partial volume effects and by spillover of tracer from tissue to blood. Three blood samples which are acquired during the second phase and are free of both partial volume and spillover effects are used to obtain a fit of an exponential form not used in previous studies. The fitting procedure uses and provides a scaling factor which depends on partial volume effects during the first window. Clustering is used to identify several tissue clusters. Parameters defining the input function, brain blood volume, and micro parameters of these tissue TACs are estimated simultaneously using the three-compartmental model for FDG PET. The technique is demonstrated using data from 20 healthy

subjects. We conclude that the proposed technique yields estimates for the cerebral metabolic rate for glucose which are almost identical to those obtained by traditional arterial blood sampling.

Key words: Quantification of FDG PET, Automated Image-derived input function, Clustering, Neuroimaging.

1 Introduction

Positron emission tomography (PET) is a widely-used Neuroimaging assessment tool that assists with disease diagnosis, treatment evaluation and study of brain function. In addition to its use for qualitative assessment, PET may also be used, especially for basic research and/or treatment evaluation, to provide quantitative estimates of physiological or metabolic parameters of interest. For example quantitative [^{18}F]-fluoro deoxyglucose (FDG) PET is used to estimate the global cerebral metabolic rate for glucose (CMRGLc), or even individual kinetic rate parameters of the glucose uptake. For such quantification, the input function, the administered tracer concentration in plasma, is required. Traditionally, the input is obtained by invasive “golden standard” arterial blood sampling. This technique not only causes discomfort to the patient but also presents some medical risk; arterial thrombosis, arterial sclerosis, and ischemia to the extremity. To obviate such difficulties, several alternative methods for estimation of the input function for various tracers have been proposed by many research groups. The work presented here extends these techniques. To put the work in context, a brief overview of existing

* Corresponding author. Tel: 480-965-8002.

Email address: hb_guo@asu.edu (Hongbin Guo).

approaches follows.

Arterialized venous blood sampling, Phelps et al. (1979). To reduce the discomfort and risks associated with the blood sampling regime the relevant limb is heated and venous blood samples are collected. While pain may be somewhat reduced, there are still issues due to the requirement of frequent blood sampling and of radiation exposure.

Population-based input function for FDG, Takikawa et al. (1993) and Eberl et al. (1997). Arterial or arterialized-venous blood samples from a subject population are used to provide a fit to an analytic representation of a population-based input function. The technique assumes that the effects of variation in the input function across subjects are negligible and insignificant with respect to the estimation of the regional CMRGLc (rCMRGLc). It is validated, Eberl et al. (1997), that this estimation is appropriate for use in quantification of rCMRGLc. The population-based input function, however, may need to be created for different study populations, different diseases, and, potentially, different PET scanners. Moreover, further studies are needed to validate this method for tracers other than FDG.

Image-derived input function corrected for partial volume, Litton (1997); Liptrot et al. (2004). In the first of the two papers, for the tracer [^{11}C]-Flumazenil, regions of interest (ROIs) containing the internal carotid artery (CA) are initially identified from the magnetic resonance images (MRI). The CA-ROI is then copied over to PET, via coregistration of MRI to PET image, in order to obtain an image-derived blood time activity curve (IBTAC). The second paper suggests instead the use of the clustering-rendered vasculature TAC for a study with the tracer [^{18}F]-altanserin. The IBTAC derived by either of these approaches is then subjected only to the correction of partial volume

effects, assuming the effects of spillover from tissue to blood can be ignored.

Image-derived input function corrected for partial volume and spillover,

Chen et al. (1998) and Wahl et al. (1999). In these two papers, for the tracer FDG or [^{18}F]6-fluoro-L-meta-tyrosine, it is assumed that spillover from tissue to blood, particularly at later times, should be considered together with correction for partial volume effects. For the simultaneous spillover and partial volume correction, it is supposed that the IBTAC from either the CA, Chen et al. (1998), or the venous sinuses, Wahl et al. (1999), can be expressed as a linear combination of the true input and the tissue time activity curve (TTAC) of neighboring tissue.

Simultaneous estimation of input and output, (SIME) Feng et al. (1997).

An analytic parameter-dependent representation of the input function is assumed. TTACs for different tissue ROIs are considered as a convolution with the same input function. Consequently, the parameters defining the input and the micro parameters associated with the ROIs can be estimated simultaneously. Though this approach is relatively robust to the location and number of the tissue ROIs, the manual procedure which is used to define the tissue ROIs and the associated computational expense needs to be addressed with further studies before the technique can be adopted as a feasible procedure for routine use.

Image-derived SIME, Sanabria-Bohorquez et al. (2003). Rather than the specific assumption of a parameter-dependent input satisfied for the entire time duration of the study, an alternative technique, first used for the tracer [^{11}C]-Flumazenil, assumes that the arterial ROI-derived IBTAC can be calibrated by blood samples at roughly 20, 40 and 60 minutes using least squares fitting, while still ignoring the impact of spillover from tissue to blood.

The method proposed and validated in this study is also an image-derived SIME technique. Initially, blood vessel CA-ROIs are identified via a semi-automated procedure in order to identify the IBTAC from blood. Then, in estimating the IBTAC, it is assumed that there are two phases of the input function. For the first short time window spillover from tissue to blood regions can be ignored because the initial uptake of the tracer by the tissue is essentially insignificant, and the input is estimated using a partial volume-corrected estimate of the IBTAC. For the remaining time interval, a large time window on the input function, spillover from surrounding tissues and partial volume effects contaminate the IBTAC from the CAs. Instead three blood samples are used to fit the input function with an exponential analytic representation. Continuity of the input is imposed at the point common to both windows. Clustering applied to the ROIs of tissues neighboring the CA-ROIs yields representative independent TTACs of these ROIs. Micro parameters of the neighboring TTACs are simultaneously estimated with parameters defining the input function.

In the remainder of the paper details of the method are presented in Section 2, validation results for data from 20 healthy subjects presented in Section 3, a discussion of implementation details in Section 4 and conclusions in Section 5.

2 Algorithm Development

2.1 Data acquisition

PET data collection for 20 healthy subjects, each with the same scanning protocol, was performed on the 951/31 ECAT (Siemens, Knoxville, TN) for

which reconstructed images are obtained by a filtered back projection algorithm. Prior to scanning 10 mCi FDG was administered. Each reconstructed data set includes 31 slices of 128×128 voxels at a resolution of approximately 9.5mm FWHM and 3.375mm separation between slices. The scanning time durations, given in minutes, for the reconstructed frames are 0.2, 8×0.0333 , 2×0.1667 , 0.2, 0.5, 2×1 , 2×1.5 , 3.5, 2×5 , 10 and 30. Sequential arterial blood samples were drawn every 5 seconds for the first minute, every 10 seconds for the second minute, every 30 seconds for the next 2 minutes, and then at 5, 6, 8, 10, 12, 15, 20, 25, 30, 40, 50 and 60 minutes, yielding a discrete representation of the blood sampled function, denoted by $u_{\text{bs}}(t_j)$, for $j = 1, \dots, 34$.

2.2 Estimation of the average image-derived blood time activity curve (AIB-TAC)

Images for the initial time frames up to time 2 minutes are integrated such as to emphasize those voxels which show occurrence of tracer in blood regions including the CA. The two dimensional blood vessel CA-ROIs \mathcal{B}_l , $l = 1 \dots p$, for these voxels are defined following the procedure described in Chen et al. (1998). While reviewing all slices over which the CA is visible, the center of each visible \mathcal{B}_l is manually identified by a single mouse click. A square \mathcal{D}_l of side 15 voxels is then automatically drawn around the center click. \mathcal{B}_l is identified as the region containing those voxels for which intensity is greater than 80% of the maximum intensity within \mathcal{D}_l , see Figure 1, and is accepted as a valid blood ROI if it has size greater than a cut-off size 10 voxels. The average of the IBTACs of the \mathcal{B}_l , the AIBTAC, $\tilde{u}(t)$ is calculated from the IBTAC of the valid blood ROIs, see Figure 2 and Figure 3. Notice that dependent on slice, one may expect at most 2 interesting CA-ROIs per slice. In general, there

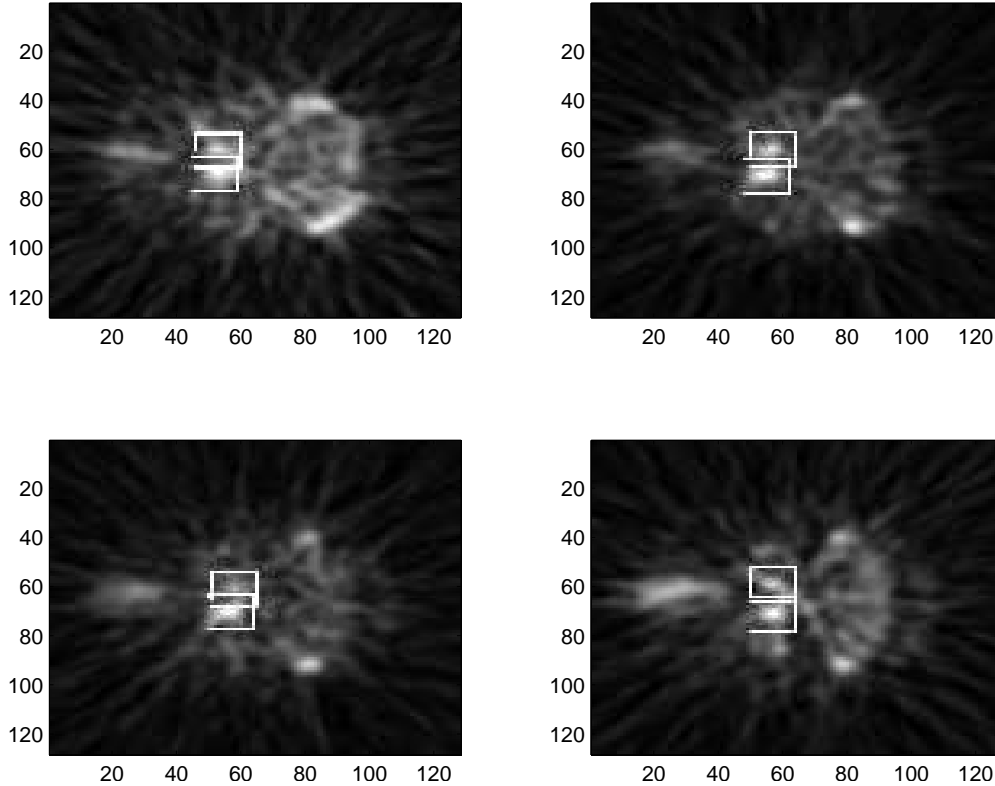


Fig. 1. Example image of the summed frames over the first two minutes, and, in the center of the images, are the semi-automatically defined squares identifying the blood regions of interest. Shown are slices 25 to 28 for subject 0827.

are no CA-ROIs toward the top of the brain. Hence the number of CA-ROIs used is typically in the range 4 – 16 for the entire brain volume.

2.3 Expression for the input function $u_e(t)$

As illustrated in Figure 3 there are two distinct phases of the AIBTAC. In the initial sub window $W_1 = [0, \tau]$, typically $\tau < 0.5$, the AIBTAC, virtually uncontaminated by spillover of tracer from surrounding tissue to blood, only needs correction due to partial volume effects. Thus, W_1 provides crucial subject and situation dependent information on the input function, specifically the time at which the tracer peaks in blood τ_p , and the time τ_0 at which the

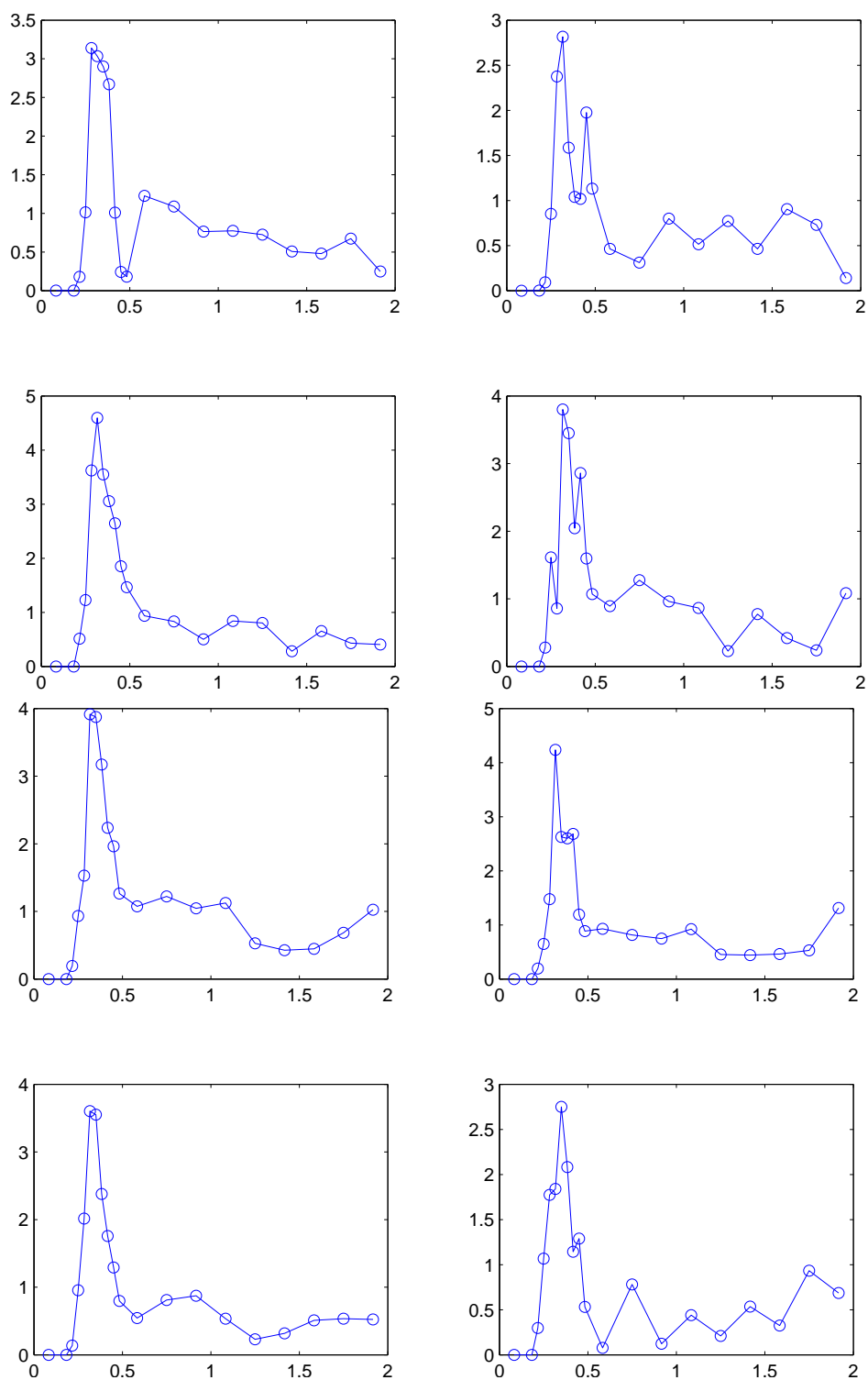


Fig. 2. The early portion of IBTACs corresponding to each of the eight CA-ROIs for the images shown in Figure 1.

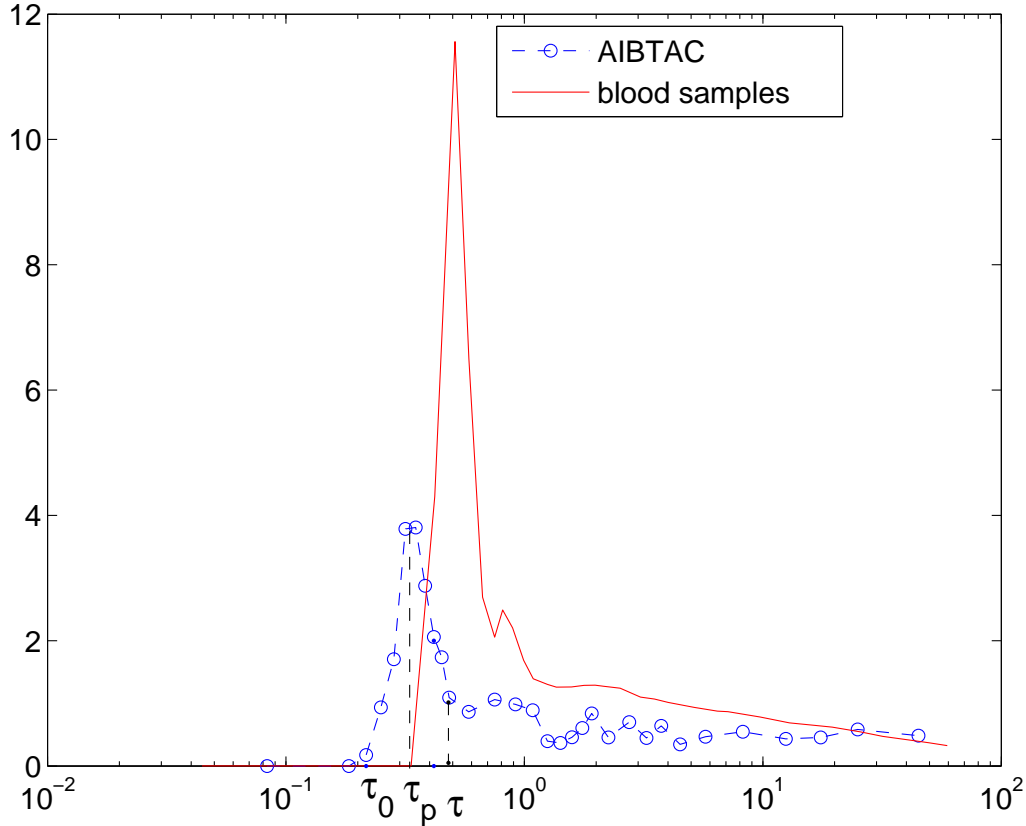


Fig. 3. Comparison of the arterial blood samples (solid red line) to un-corrected AIBTAC (blue circles) and the illustration of the determination of peak location, the time point which separates the fast and slow phases, and the time at which blood tracer activity has been initiated. Time is expressed on logarithm scale. These two curves clearly demonstrate the apparent partial volume and spillover effects especially on the later time window.

tracer reaches the blood ROI in the brain. Notice that this point τ_0 is shifted relative to time of tracer administration because of the very slight time delay between time of administration of tracer and its arrival in the brain, and must therefore be estimated for the later cluster analysis. On the later time window $W_2 = [\tau, T]$, it is assumed that the impact of spillover on $\tilde{u}(t)$ is not negligible and $\tilde{u}(t)$ does not demonstrate a smooth exponential decay of tracer in blood as would be expected.

For W_1 , first τ_p is determined automatically as the point at which the highest intensity value $\tilde{u}(\tau_p)$ is achieved. Various methods are available to estimate the delay time τ_0 , Raichle et al. (1983). Here τ_0 , prior to which the signal to noise ratio (SNR) is very poor, is selected automatically as the point after which $\tilde{u}(t)$ remains greater than 2% of the peak value $\tilde{u}(\tau_p)$. Values of $u_e(t)$ prior to time τ_0 are set identically to 0. Finally, τ can be chosen in a variety of ways. In the results reported here, τ is actually selected manually by visual examination of the AIBTAC, but other choices have been verified. For example, a simple choice is to find the time point of the AIBTAC which is closest to $2\tau_p - \tau_0$ so that τ is symmetrically chosen relative to the peak. An automatic approach which is more objective uses a fitting of the AIBTAC data over a time interval $[\tau_p, \tau_a]$ where τ_a is chosen automatically such as to include the range of the AIBTAC during which the rapid washout of tracer occurs, and then to find τ as the point of inflection of this fitted curve. The choice of τ also needs to account for the tracer activity in the surrounding tissue.

Now, supposing that $\tilde{u}(\tau)$ is known, the approximate value of the AIBTAC on window W_1 may be simply estimated by the piecewise linear interpolation \tilde{u}_1 to \tilde{u} and the estimated input on W_1 is $u_e(t) = c_1\tilde{u}_1$, where c_1 is the unknown recovery coefficient which accounts for correction due to partial volume effects on the initial window. For W_2 it is assumed that the input function decays exponentially after time τ according to $u_e(t) = c_1\tilde{u}_1(\tau) \exp(-\gamma(t - \tau)^\delta)$, where γ and δ are unknown parameters.

Specifically, in terms of all parameters the estimated form of the input function

is given by

$$u_e(t, c_1) = c_1 \begin{cases} 0 & t \leq \tau_0, \\ \tilde{u}(\tau_p) \frac{(t-\tau_0)}{(\tau_p-\tau_0)} & \tau_0 < t \leq \tau_p \\ \tilde{u}(\tau_p) \frac{(\tilde{u}(\tau)/\tilde{u}(\tau_p))(t-\tau_p)+(\tau-t)}{(\tau-\tau_p)} & \tau_p < t \leq \tau \\ \tilde{u}(\tau_p) \left(\frac{\tilde{u}(\tau)}{\tilde{u}(\tau_p)} e^{-\gamma(t-\tau)^\delta} \right) & t > \tau \end{cases}. \quad (1)$$

Notice that continuity at τ is imposed, and that the factoring by the ratio $\tilde{u}(\tau)/\tilde{u}(\tau_p)$ is useful in demonstrating the dependence of u_e on both the peak value and the recovery coefficient c_1 .

Given a value for the recovery coefficient, unknown parameters γ and δ can be obtained by the fit of u_e to the exponential form $(\tilde{t}_l, u_{\text{bs}}(\tilde{t}_l))$ where blood sampled data, $u_{\text{bs}}(\tilde{t}_l)$, $l = 1, \dots, 3$, are obtained for $\tilde{t}_1 \approx 10$, $\tilde{t}_2 \approx 30$ and $\tilde{t}_3 \approx 60$. The fit is carried out stably using both scaling of the blood samples by the common factor $c_1 \tilde{u}(\tau_p)$ and using the equivalent logarithmic expression. Moreover, for any choice of c_1 the fit is initialized with $\delta = 1$ and an easily derived explicit expression for γ when $\delta = 1$.

2.4 Clustering the tissue time activity curves (TTACs)

For each valid blood ROI \mathcal{B}_l a region of neighboring tissues \mathcal{N}_l is identified by taking all tissue voxels which are a distance d from \mathcal{B}_l , where $0.5 \text{ FWHM} \leq d \leq 2 \text{ FWHM}$, measured in three dimensions. The clustering method described in Guo et al. (2003) is utilized to cluster to m groups all TACS from the \mathcal{N}_l . Average TTACs for each of the cluster groups, denoted by $y_i^{\text{TAC}}(t)$, $i = 1, \dots, m$ provide m independent representative TACs for the neighboring

tissues and may be used for the simultaneous estimation of input function parameters and micro parameters for the neighboring tissue TACs. Typically, m is in the range 3–5 which reflects the number of significant physiologically different tissue groups that can be recognized by clustering.

2.5 Simultaneous estimation of the input function

In the three-compartmental model Sokoloff et al. (1977) for FDG PET, the output $y(t)$ at a given voxel, or for a specific ROI, is given analytically by convolution (\otimes) of the instantaneous response function (IRF) with the input $u(t)$

$$y(t) = u(t) \otimes \left(\frac{K_1 k_3}{k_2 + k_3} + \frac{K_1 k_2}{k_2 + k_3} e^{-(k_2 + k_3)t} \right). \quad (2)$$

Here the IRF is the term within the parentheses and is dependent on voxel location through the kinetic parameters, K_1 is the transport rate from blood to extra-vascular space, k_2 is the transport rate back from extra-vascular space to blood, and k_3 is the phosphorylation rate of intra-cellular FDG by hexokinase enzymes to FDG-6-phosphate. In this study, it is assumed that the dephosphorylation rate of intra-cellular FDG-6-phosphate back to FDG k_4 is identically zero, because it is relatively very small and the scanning duration of 60 minutes is not long enough to provide a reliable estimate of k_4 , Huang et al. (1980). From this expression, and ignoring spillover effects, the voxel or ROI micro parameters are then typically estimated by a nonlinear (NL) fit of measured TAC $y^{\text{TAC}}(t)$ to $y(t)$, assuming knowledge of $u(t)$, traditionally using the blood sampled data $u_{\text{bs}}(t)$ for the entire scan duration.

Here, given the representative clustered TTACS of the tissues neighboring the CAs, $y_i(t) \approx y_i^{\text{TAC}}(t)$, $i = 1 \dots m$, $m \geq 2$, the weighted nonlinear least squares (WNLS) cost function in terms of the unknown parameters c_1 and $K_1^{(i)}$, $k_2^{(i)}$, $k_3^{(i)}$, $i = 1 \dots m$, all included in parameter vector \mathbf{x} , and vector α the vector of unknowns α_i , $i = 1 \dots m$, is

$$\Phi(\mathbf{x}, \alpha) = \sum_{i=1}^m \sum_{j=1}^n w_j \left[y_i^{\text{TAC}}(t_j) - \alpha_i \cdot y_i(t_j) - (1 - \alpha_i) \cdot u_e(t_j, c_1) \right]^2. \quad (3)$$

The weight w_j is set to the time duration of each frame, and parameters α_i correct for local spillover from blood to tissue. The constrained global fit is then

$$\begin{aligned} \min_{\mathbf{x}, \alpha} \Phi(\mathbf{x}, \alpha) \quad \text{subject to} \quad & 1.2 \leq c_1 \leq 4 \quad 0.9 \leq \alpha_i \leq 1 \\ & 0.015 \leq K_1^{(i)} \leq 0.3, \quad 0.024 \leq k_2^{(i)} \leq 0.54, \quad 0.01 \leq k_3^{(i)} \leq 0.2. \end{aligned} \quad (4)$$

The bound constraints on the micro parameters are based on experimental results Huang et al. (1980) for both gray and white matter from 13 healthy subjects, but with doubling of upper bounds and halving of lower bounds so as to not provide bounds which may be too conservative. Note that the tissue TACs y_i^{TAC} are shifted to match the activity start time τ_0 of the AIBTAC.

Matlab function “*fmincon*” which uses a sequential quadratic programming (SQP) method for a medium scale problem of this kind, is used to solve the constrained optimization problem.

3 Results

3.1 Qualitative comparison for the input function

A comparison of the estimated input function u_e , after solution of (4) to find c_1 , with the blood-sampled input u_{bs} is illustrated in Figure 4. The upper figure presents the portion within 1.5 minutes, and the middle figure the curves for the whole time duration, 45 minutes, on the logarithmic scale. Because these two curves come from different sources, namely estimation and actual blood samples, there is a time shift between them. In order to provide better comparison u_{bs} is shifted to match u_e , see the lower plots in Figure 4. As expected the tails of both curves are closer because the tail of the estimated curve is obtained by the fit with the blood samples. For almost all subjects $u_e(t)$ is smoother for later time because it is evaluated using the analytic exponential form. Representative comparisons of u_e with shifted u_{bs} selected from the 20 subjects are shown in Figure 5. The heights of the peaks $u_e(\tau_p)$ match well in all cases, with differences in peak always less than 20%. Moreover, in some cases it can be assumed that the estimated heights of u_e are more reliable than those of u_{bs} due to the potential for low resolution around the peak, see for example, subject 1227.

3.2 Quantitative validation

For each subject, micro parameters associated with the tissue TACs of gray matter are calculated using the blood-sampled input function and the estimated input from the SIME optimization. Regression analyses comparing estimations of parameters K_1 , k_2 , k_3 and K are illustrated in Figure 6. While

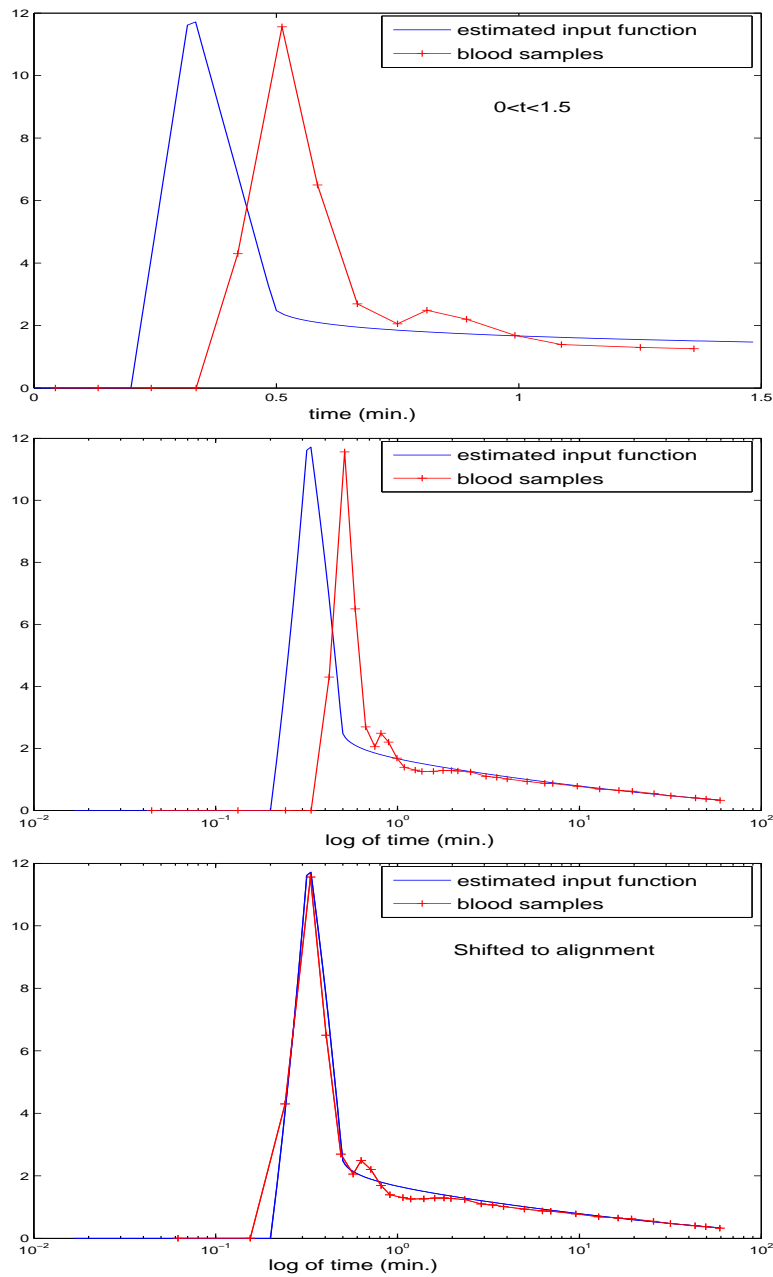


Fig. 4. The input function estimated by proposed method compared with arterial blood samples. Illustrated are the data focused on the initial window (top panel), the whole time window given on logarithm scale (middle panel), and the same data with the estimated input shifted to account for the time delay relative to the blood samples (bottom panel).

Table 1

Parameters calculated using the estimated input after carrying out the SIME (4). The results are u_{bs} / u_e and the maximum of the relative errors: $\max_{i=1,\dots,3} |x_i^{bs} - x_i| / |x_i^{bs}|$, $x_1 = K_1$, $x_2 = k_2$, $x_3 = k_3$, where x^{bs} represents the values from blood sample data, and x is the value obtained using the SIME-estimated input function. Worst cases are highlighted.

Subject	K_1	k_2	k_3	max err %
1206	0.131 / 0.136	0.052 / 0.056	0.062 / 0.064	8.7
1227	0.121 / 0.107	0.122 / 0.111	0.051 / 0.057	13.6
817	0.110 / 0.141	0.151 / 0.153	0.089 / 0.064	28.2
1154	0.090 / 0.090	0.071 / 0.075	0.055 / 0.060	8.91
1208	0.102 / 0.097	0.076 / 0.080	0.060 / 0.071	17.7
1231	0.116 / 0.150	0.091 / 0.093	0.065 / 0.049	29.7
1245	0.120 / 0.122	0.126 / 0.139	0.070 / 0.075	10.9
827	0.113 / 0.103	0.118 / 0.099	0.067 / 0.069	15.7
1182	0.094 / 0.100	0.050 / 0.051	0.037 / 0.037	5.7
1226	0.116 / 0.138	0.077 / 0.086	0.036 / 0.032	19.8
1233	0.113 / 0.132	0.080 / 0.085	0.060 / 0.048	20.5
1264	0.108 / 0.128	0.070 / 0.100	0.055 / 0.061	43.0
1078	0.109 / 0.098	0.106 / 0.082	0.088 / 0.091	22.3
1234	0.192 / 0.147	0.262 / 0.193	0.115 / 0.128	30.2
1086	0.097 / 0.095	0.094 / 0.103	0.051 / 0.059	16.1
1191	0.114 / 0.124	0.041 / 0.049	0.047 / 0.050	18.7
1235	0.117 / 0.141	0.123 / 0.125	0.056 / 0.045	19.8
1121	0.087 / 0.090	0.057 / 0.056	0.038 / 0.036	5.6
1229	0.088 / 0.098	0.040 / 0.067	0.047 / 0.065	67.4
1241	0.102 / 0.105	0.144 / 0.129	0.087 / 0.074	14.9

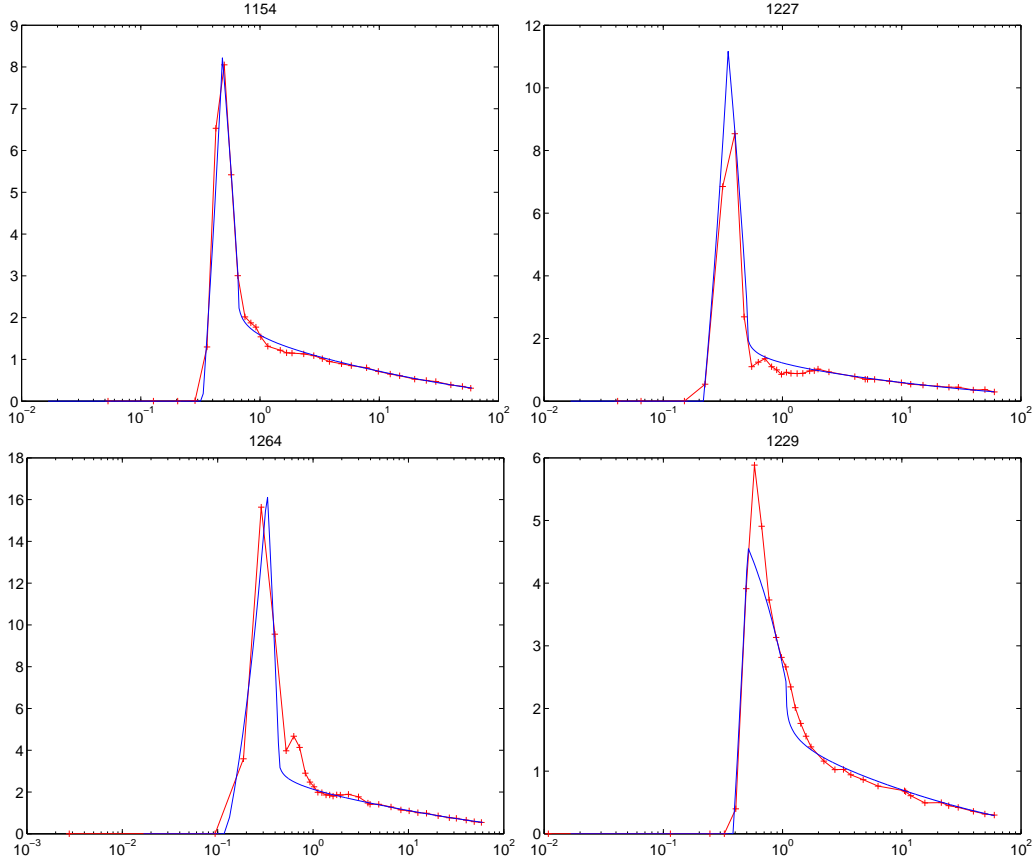


Fig. 5. Comparison of estimated input u_e , continuous line (blue), and blood-sampled input u_{bs} , crosses (red), for representative subjects including the two worst cases 1229 and 1264.

the estimation for K is almost perfect, the slope for the fit for k_3 is much better than that for K_1 and k_2 , although the correlation coefficient for the fit for k_3 is not so good as that for k_2 . Thus in order to better understand the relationship between the two sets of values, the relative errors for parameters K_1 , k_2 , k_3 and K are also considered. The means of these relative errors are, resp., 0.055, 0.053, 0.0097 and -0.02 , while the standard deviations are 0.139, 0.209, 0.168 and 0.019. The specific parameters in each case are presented in Table 1.

Careful examination of the data for the subjects with the worst results, indi-

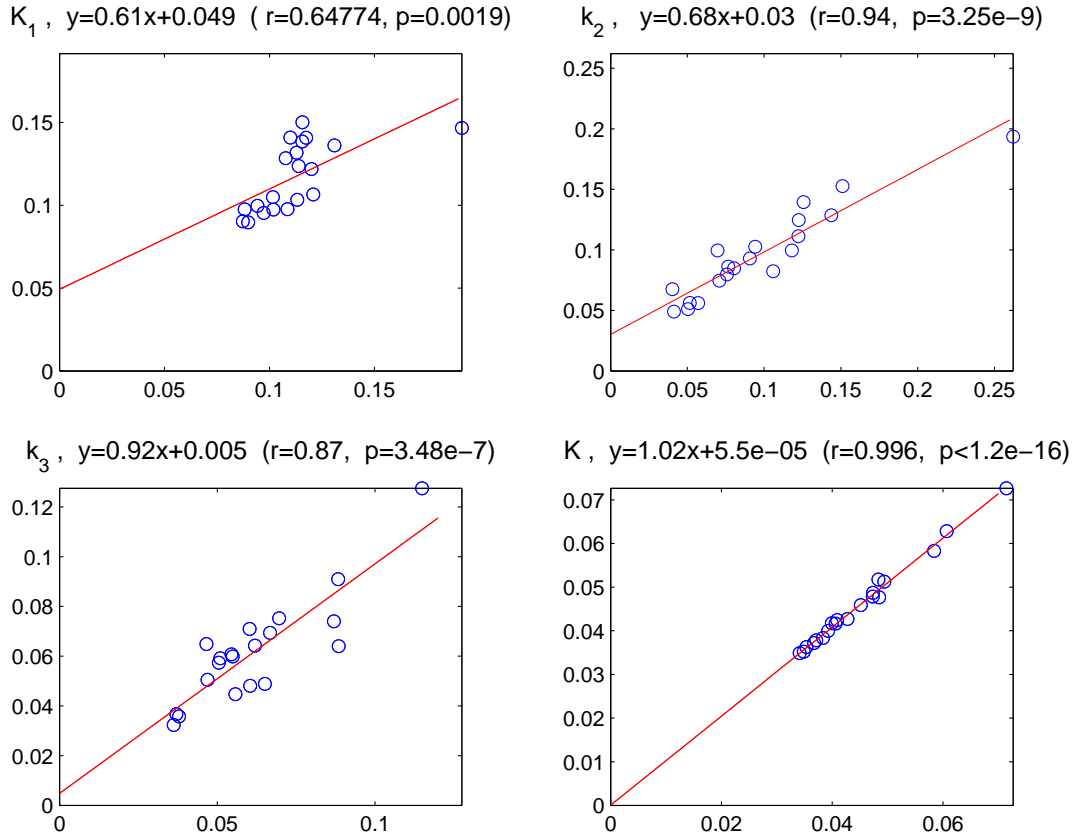


Fig. 6. Comparing the two sets of parameters calculated by the estimated and the blood sampled inputs.

cates that the early blood samples (from 1 to roughly 10 minutes) demonstrate lower SNRs. The worst results which are highlighted in the table are associated with subjects 1264, 1229, 1234, 1231 and 0817. Note that in no case do the constraints reach their bounds, suggesting that the chosen bounds are quite appropriate in the context of this analysis.

4 Discussion

The basic idea of the proposed method is the consideration of the two phases of the input function. For the period of fast rapid accumulation followed by fast

washout the input is derived from the average blood ROI TAC. For the later period a few blood samples are used to provide an analytic exponential fit to the data rather than rely on blood ROI with possible low SNR. Simultaneous estimation of tissue TAC micro parameters and parameters defining the input are obtained by nonlinear minimization of a constrained cost function derived for the standard three-compartmental model of FDG PET. The tissue micro parameters for gray tissue TACs are then post estimated using the estimated input. Additional implementation considerations and details follow.

4.1 Choice of blood ROIs and IBTACs

After summing the early frames it is generally easy to see the CAs from the bottom slices. Slices in which the blood ROIs are not clear or are very small are ignored. On the other hand, a clear ROI does not necessarily mean that the IBTAC is good because in some cases the early data of the selected ROI have poor SNRs. Thus only slices with good IBTAC ROIs are selected for the analysis. The method has also been tested using the blood vessel ROIs of the superior sagittal sinus (SSS). Note, because of anticipated differences between blood in the artery and the sinus, in these tests the two types of IBTAC are not mixed. Specifically, in the selection stage for generation of the average IBTAC, the ROIs used are chosen either from the sinuses or artery, but not from both. Generally, the size of CA is smaller than that of the SSS, and the IBTACs of the former ROI have lower peaks. The difference between the peaks is then accounted for by the value of the recovery coefficient, see (1), which is calculated by the SIME, and no significant differences between final results by either approach are recognized. Of most importance is that the selected IBTACs from either kind of ROI have the best SNRs possible.

4.2 Separation of early and late phases of the input function

The estimation of τ , which separates the early rapid accumulation plus fast washout phase of tracer in the input function from the period of exponential decay of tracer, is crucial, but as already noted can be easily defined automatically or by manual selection. Its significance is to assure that the most reliable data are used for each window. In the early window, partial volume effects assure that the peak of the input will not be recognized in the blood ROIs, regardless of choice of SSS or CA. The SIME process, however, optimizes with respect to the recovery coefficient which directly scales the peak (1) and thus is also sensitive to misspecification of the peak value. The use of the linear interpolation for the early phase is a crude simplification, but in the nonlinear estimation the weights applied to this data are very small, and it is most significant that the peak and the area under the curve are well approximated. Clearly, it is also possible to use higher order fitting Eberl et al. (1997) rather than linear interpolation for this early phase, but the end result will be insignificant, particularly for a code which uses a composite trapezoidal rule for numerical integration of the convolution integral. On the other hand, for later time, when exponential decay sets in, but for which spillover from tissue to blood may contaminate the AIBTAC, blood samples are utilized to obviate this difficulty.

Other formulations for the analytic representation of the input were considered, Eberl et al. (1997); Wong et al. (2001), in this work, but the specific formulation utilized here performed best for the data considered. In particular, in the tests it is evident that δ is in the range 0.3–0.5 rather than close to 1.

4.3 *Fitting formulation*

In order to provide reasonable solutions in a cost effective manner, it is important that bounds on the parameters of the nonlinear minimization are provided. Increasing the number of unknowns defining the input function quickly raises the complexity of the NLS optimization through the dependence of the analytic fit also on the input parameter. It is thus clear that the expression in terms of one very dominant factor (1), the product of the peak value and the recovery coefficient, makes SIME viable. The clustering assures that the TTACs used in the SIME are related to ROIs with consistent voxels. Finally, while different weights in the NLS might lead to differences, experiments with the square root of the time duration, or the unweighted case, give inferior results.

5 **Conclusion**

A reliable semi-automated alternative for input function estimation, which keeps number of blood samples, indeed arterial blood samples, to a minimum, has been presented and validated with consistent FDG PET analysis from 20 healthy subjects. Macro parameter K , and micro parameters, K_1 , k_2 and k_3 are well estimated as compared to the use of traditional blood sampling. Because of the generality of the approach, and its relative simplicity for implementation, the proposed method should also work for other tracers. The Matlab-based implementation of the tool is available at web site <http://math.asu.edu/~hongbin>. For future work it is planned to further refine the approach to estimate parameter k_4 and to use pharmacokinetic analysis of

the tracer input for estimation of the input peak value, such as to possibly separate the estimation of the input from that of the kinetics of the data. It is also of interest to validate the method for use with small animal studies (microPET), Huang et al. (2004).

6 Acknowledgments

This work was partially supported by the Arizona Center for Alzheimer's Disease Research which is funded by the Arizona Department of Health Services, and by NIH grant EB 2553301.

References

- Chen, K., Bandy, D., Reiman, E., Huang, S.-C., Lawson, M., Feng, D., Yun, L.-S., Palant, A., 1998. Noninvasive quantification of the cerebral metabolic rate for glucose using positron emission tomography, 18F-fluorodeoxyglucose, the Patlak method, and an image-derived input function. *J. Cereb. Blood Flow Metab.* 18, 716–723.
- Eberl, S., Anayat, A. R., Fulton, R. R., Hooper, P. K., Fulham, M. J., 1997. Evaluation of two population based input functions for quantitative neurological FDG PET studies. *Eur. J. Nucl. Med.* 24, 299–304.
- Feng, D. G., Wong, K.-P., Wu, C.-M., Siu, W.-C., 1997. A technique for extracting physiological parameters and the required input function simultaneously from PET image measurements: Theory and simulation study. *IEEE Trans. Inform. Technol. Biomed.* 1 (4), 243–254.

- Guo, H., Renaut, R., Chen, K., Reiman, E., 2003. Clustering huge data sets for parametric PET imaging. *Biosystems* 71 (1-2), 81–92.
- Huang, S.-C., Phelps, M. E., Hoffman, E. J., Sideris, K., Selin, C. J., Kuhl, D. E., 1980. Noninvasive determination of local cerebral metabolic rate of glucose in man. *Am. J. Physiol.* 238 (E), 69–82.
- Huang, S.-C., Wu, H.-M., Shoghi-Jadid, K., Stout, D. B., Chatziioannou, A., Schelbert, H. R., Barrio, J. R., 2004. Investigation of a new input function validation approach for dynamic mouse micropet studies. *Molecular Imaging and Biology* 6 (1), 34–46.
- Liptrot, M., Adams, K. H., Martiny, L., Pinborg, L. H., Lonsdale, M. N., Olsen, N. V., Holm, S., Svarer, C., Knudsen, G. M., 2004. Cluster analysis in kinetic modelling of the brain: a noninvasive alternative to arterial sampling. *Neuroimage* 21 (2), 483–493.
- Litton, J.-E., 1997. Input function in PET brain-studies using MRI defined arteries. *J. Comp. Ass. Tom.* 21 (6), 907–909.
- Phelps, M. E., Huang, S. C., Hoffman, E. J., Selin, C. E., Kuhl, D., 1979. Tomographic measurement of local cerebral glucose metabolic rate in man with (^{18}F) fluorodeoxyglucose: Validation of method. *Ann. Neurol.* 6, 371–388.
- Raichle, M., Martin, W., Herscovitch, P., Mintun, M., Markham, J., 1983. Brain blood flow measured with intravenous H_2O^{15} ii. implementation and validation. *J. Nucl Med* 24, 790–798.
- Sanabria-Bohorquez, S. M., Maes, A., Dupont, P., Bormans, G., de Groot, T., Coimbra, A., Eng, W., Laethem, T., Lepeleire, I. D., Gambale, J., Vega, J. M., Burns, H. D., 2003. Image-derived input function for [^{11}C] flumazenil kinetic analysis in human brain. *Mol. Imag. Biol.* 5 (2), 72–78.
- Sokoloff, L., Reivich, M., Kennedy, C., Rosiers, M. H. D., Patlack, C. S., Pet-

- tigrew, K. D., Sakurada, M., Shinohara, M., 1977. The [^{14}C] deoxyglucose method for the measurement of local cerebral glucose metabolism: theory procedures and normal values in the conscious and anesthetized albino rat. *J. Neurochem.* 28, 897–916.
- Takikawa, S., Dhawan, V., Spetsieris, P., Robeson, W., Chaly, T., Dahl, R., Margouloff, D., Eidelberg, D., 1993. Noninvasive quantitative fluorodeoxyglucose PET studies with an estimated input function derived from a population-based arterial blood curve. *Radiology* 188, 131–136.
- Wahl, L. M., Asselin, M. C., Nahmias, C., 1999. Regions of interest in the venous sinuses as input functions for quantitative PET. *J. Nucl. Med.* 40 (10), 1666–1675.
- Wong, K.-P., Feng, D., Meikle, S. R., Fulham, M. J., 2001. Simultaneous estimation of physiological parameters and the input function - In vivo PET data. *IEEE Trans. Inform. Technol. Biomed.* 5 (1), 67–76.